ACS NANO

www.acsnano.org

ARTICLE

Cracking of Polycrystalline Graphene on Copper under Tension

Seung Ryul Na,[†,§] Xiaohan Wang,[‡,§] Richard D. Piner,[‡] Rui Huang,[†] C. Grant Willson,[‡] and Kenneth M. Liechti*[,†]

[†]Department of Aerospace Engineering and Engineering Mechanics, Research Center for the Mechanics of Solids, Structures and Materials, and [‡]The Materials Science and Engineering Program, The University of Texas at Austin, Austin, Texas 78712, United States

Supporting Information

ABSTRACT: **Roll-to-roll manufacturing of graphene is attractive because of its compatibility with flexible substrates and its promise of high-speed production. Several prototype roll-to-roll systems have been demonstrated, which produce large-scale graphene on polymer films for transparent conducting film applications.[1−4] In spite of such progress, the quality of graphene may be influenced by the tensile forces that are applied during roll-to-roll transfer. To address this issue, we conducted *in situ* tensile experiments on copper foil coated with graphene grown by chemical vapor deposition, which were carried out in a scanning electron microscope. Channel cracks, which were perpendicular to the loading direction, initiated over the entire graphene monolayer at applied tensile strain levels that were about twice the yield strain of the (annealed) copper. The spacing between the channel cracks decreased with increasing applied strain, and new graphene wrinkles that were parallel to the loading direction appeared. These morphological features were confirmed in more detail by atomic force microscopy. Raman spectroscopy was used to determine the strain in the graphene, which was related to the degradation of the graphene/copper interface. The experimental data allowed the fracture toughness of graphene and interfacial properties of the graphene/copper interface to be extracted based on classical channel crack and shear-lag models. This study not only deepens our understanding of the mechanical and interfacial behavior of graphene on copper but also provides guidelines for the design of roll-to-roll processes for the dry transfer of graphene.**

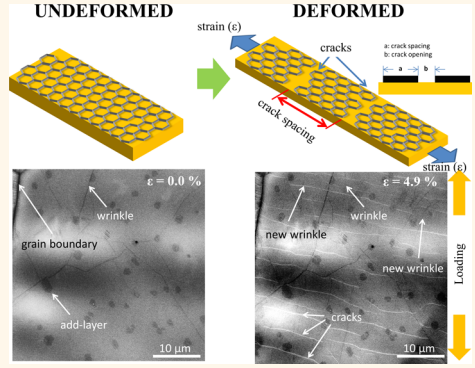

KEYWORDS: *graphene, channel cracks, fracture energy, stress transfer, interfacial shear stress*

Graphene is a two-dimensional material with a host of potential applications such as flexible touch screens,[1] solar panels,[5] and membranes to desalinate and purify water.[6] However, using graphene in such applications requires large-scale and cost-effective methods for graphene synthesis and processing.[7] Recently, a chemical vapor deposition (CVD) method was developed,[8] which enabled growth of uniform monolayers of graphene on copper foil. This method overcame the size limitation of graphene synthesis as it can, in principle, be performed with copper substrates of any size. Currently, the CVD graphene is transferred from the copper foil to target substrates by etching away the copper[9] or by an electrochemical process,[10] which uses the bubbles generated to lift the graphene off the copper.

Roll-to-roll (R2R) processes are particularly suitable as they enable continuous processing and transfer of graphene.[3,4,11] Two essential R2R processes have been developed for graphene in the past few years: CVD growth of graphene on moving copper foils[2,4,12] and transfer of graphene from the copper surface onto flexible substrates.[1−4] However, it appears that these attempts at R2R transfer led to polymer/graphene films with relatively high sheet resistance. The hypothesis of the current work is that the tensile forces that are required for R2R processes could lead to cracking of the graphene.

In the early stages of graphene research, the mechanical properties of single-crystal graphene were primarily studied by indentation with atomic force microscopes (AFM)[13] and molecular dynamics (MD) simulations.[14−16] It was found that graphene is a very stiff (1 TPa Young's modulus), strong (130 GPa tensile strength),[13] and ductile material (20% failure strain).[17] For AFM indentation, graphene was obtained by peeling monolayers off graphite with scotch tape, which resulted in very small samples. On the other hand, CVD graphene monolayers are much larger and polycrystalline and have numerous atomic defects and grain boundaries.[18,19] From

Received: July 29, 2016
Accepted: September 21, 2016
Published: September 21, 2016

DOI: 10.1021/acsnano.6b05101
ACS Nano 2016, 10, 9616−9625

a fracture mechanics perspective, such defects are expected to reduce failure strains. Indeed, it was recently reported that the tensile strength and strain to failure of CVD graphene were 2−3 GPa and 0.2−0.3% strain, respectively.[20] Such brittle fracture may also occur in the R2R processing of CVD graphene, and guidelines are therefore required for the successful processing of graphene using this approach.

Such effects may be modulated by the behavior of the interface between the graphene and copper and the potential for sliding. For example, when a polymer film with graphene transferred to it was subjected to small strains (<0.5%), the deformation through the thickness of the bilayer was uniform.[21−25] However, at larger strains, there was slippage between the two films.[22−24] It was also observed that graphene buckle delaminations were induced when the stretched film was released.[23] These phenomena may carry over to the R2R transfer of graphene.

In this work, a method was developed to study the tensile response of graphene grown on copper foil. *In situ* SEM tensile testing established that graphene cracked at a relatively low levels of applied strain (~0.44%) and formed new wrinkles parallel to the loading direction. Further details of these morphological changes in graphene were provided by AFM and Raman spectroscopy. A fracture mechanics analysis of channel cracking and a shear-lag model were adopted to interpret the data, which allowed the fracture toughness of graphene and the properties of the interface between graphene and copper foil to be established.

RESULTS AND DISCUSSION

High-quality monolayer graphene was grown on strips of copper foil (Figure S1b) using a low-pressure chemical vapor deposition system.[8] A microtensile tester (Figure S1a) (Deben Inc.) was mounted on the *XYZ* stage of an FEI Quanta 600 scanning electron microscope (SEM). Each graphene-coated strip was mounted in the clamping blocks, which were aligned with the shoulders of the samples in order to maintain a consistent gage length (Figure S1b,c). The tensile load was applied under displacement control at a rate of 1.67 μm/s, while the load was measured with a load cell. The relative displacement of the gripping assembly was measured with a linear variable differential transformer. This provided a global measure of deformation that included the deformation of the grips and the specimen. The actual displacement in the specimen was obtained by calibrating the stiffness of the gripping assembly and subtracting out its deformation (see Supporting Information). The loading was interrupted at 10 N intervals in order to allow SEM images to be captured over the complete strain range, typically up to 10%.

Schematics of graphene in the undeformed state and at 4.9% strain are shown in Figure 1, along with corresponding SEM images. Graphene wrinkles[26] and add-layers[27,28] were observed on the undeformed sample (Figure 1a); the former are presumably formed due to the difference in the coefficients of thermal expansion between graphene and the copper substrate,[8] while add-layers are due to the growth of additional graphene at the copper/monolayer graphene interface.[27,28] As an example, at an applied strain of 4.9%, it can be seen (Figure 1b) that the surface morphology of the graphene film changed significantly; a series of approximately equally spaced and parallel bright lines appeared perpendicular to the loading direction. These were cracks in graphene that exposed the underlying copper substrate.[29,30] They were confined to the

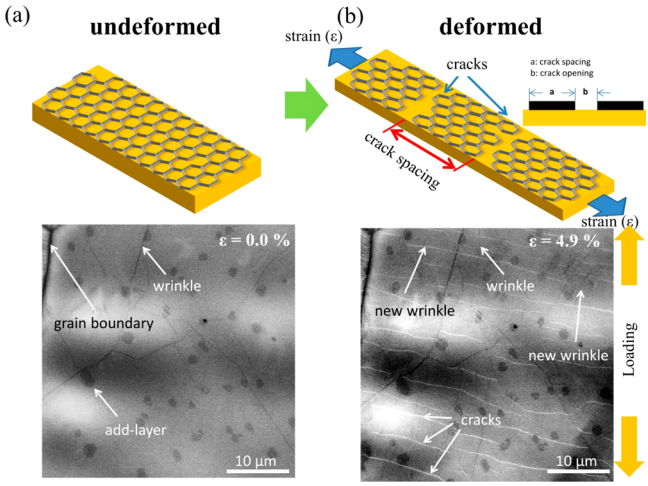

Figure 1. Schematics of graphene and SEM: (a) undeformed case and (b) deformed sample.

graphene monolayer and did not penetrate the underlying copper foil. The change in crack spacing[31] with applied strain was used to determine the fracture toughness of graphene and strength of the shear interactions between graphene and copper. It is also worth noting that new graphene wrinkles were formed during the tensile test, which were parallel to the loading direction.

Figure 2 shows time-lapsed SEM images of a graphene film during the tension test. We used snapshots at specific levels of applied strain on copper foil because it was difficult to capture SEM images while the grips were moving. No cracks were observed at zero applied strain (Figure 2a). Instead, the only features that could be observed were wrinkles and add-layers. At an applied strain of 0.44% (Figure 2b), three cracks (Ⓐ, Ⓑ, and ©) can be identified, which are perpendicular to the loading direction. This level of applied strain was identified in about eight experiments as the critical strain for the onset of channel cracking in the graphene and is about double the strain at the onset of plastic deformation of the copper foil (Figure S2). An immediate consequence of this result for designing R2R systems is that the strains in the graphene should be less than the yield strain of the copper foil.

In recent studies, graphene was transferred to polyethylene terephthalate (PET) film with ethyl vinyl acetate using R2R processes in conjunction with electrochemical delamination or delamination under hot water.[3,4] The sheet resistance of the graphene on the PET film was approximately 3000 to 6000 Ω/□. This is a factor of 4−8 times the sheet resistance of CVD graphene that was mechanically transferred to epoxy[32] and may suggest that the graphene cracked during the R2R process.

In addition, the fracture strain found here is much lower than the commonly cited failure strain of graphene (~20%). Density functional theory[33,34] and MD calculations[16,17] have predicted similarly high levels of fracture strain. However, single-crystal graphene was considered in both the experiments and analyses, whereas the CVD graphene being considered in the present study is polycrystalline and usually contains numerous defects.[19,71,73] Recently, MD simulations of polycrystalline graphene consisting of 5−10 grains within regions of several nanometers predicted fracture strains of about 5%[15,35−38] due to crack initiation at grain boundaries. A recent experiment on CVD graphene with a flaw produced by focused ion beam etching found that fracture initiated at approximately 0.25%

DOI: 10.1021/acsnano.6b05101
ACS Nano 2016, 10, 9616−9625

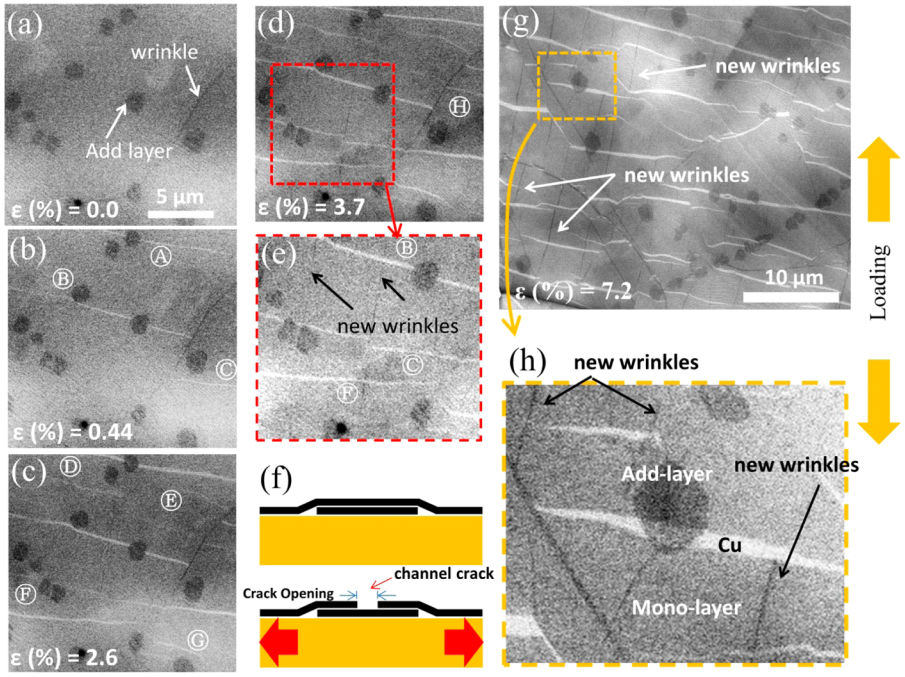

Figure 2. Time-lapsed SEM images of a graphene film during the tension test at the strain of (a) 0.0%, (b) 0.44%, (c) 2.6%, and (d) 3.7%; (e) magnified image; (f) schematic of the channel crack at the add-layer graphene; (g) 7.2%; and (h) high-resolution SEM image near the add-layer graphene.

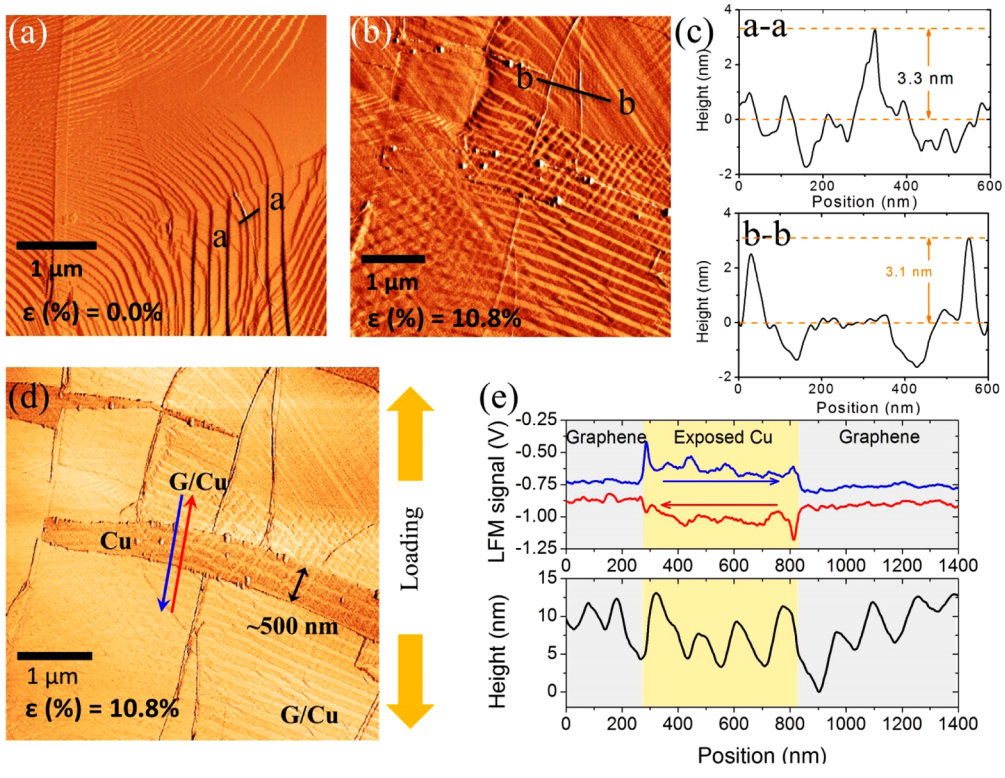

Figure 3. AFM images of undeformed and deformed graphene/copper: (a) undeformed, (b) deformed at the strain of 10.8%, (c) profiles of graphene wrinkles, (d) friction force plot obtained from lateral force microscopy, and (e) friction force and topological plot along the blue and red arrows in (d).

strain for a toughness of 16 J/m^2.[20] This is much closer to the critical strain levels encountered in the present study and supports the idea that the channel cracks initiated at defects.

Three other interesting observations can be made from the *in situ* experiments in the SEM. First, there was a characteristic spacing between the channel cracks. As will be seen later, this characteristic spacing allowed the fracture toughness of monolayer graphene and the interfacial behavior between graphene and its seed copper foil to be estimated. Second, channel cracks (*e.g.*, Ⓑ and Ⓒ) were often arrested when they

DOI: 10.1021/acsnano.6b05101
ACS Nano 2016, 10, 9616−9625

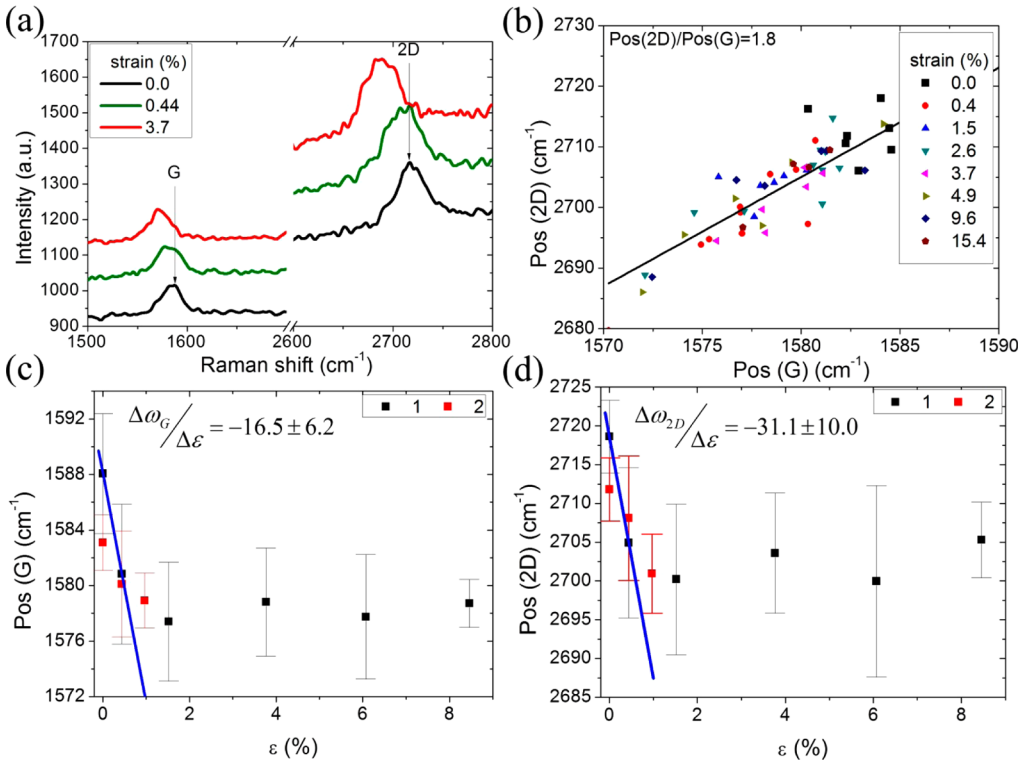

Figure 4. Raman response of graphene on the copper foil at the applied strains. (a) Raman shift of G and 2D peaks due to the applied strains, (b) correlation between 2D and G peaks at various applied strains, (c) Raman shift of the G peak by the applied strain, and (d) Raman shift of the 2D peak by the applied strain.

encountered wrinkles. This seems to be due to the fact that the wrinkles can relieve the strain at the tip of a propagating crack. The last observation is that the channel cracks such as Ⓐ and Ⓑ in the monolayer graphene did not penetrate into the add-layers beneath it. The reason for this may be related to the relatively weak interaction between the monolayer and add-layer.[39] The interlayer shear strength of graphite is relatively low at 0.03 MPa[40] and is governed by van der Waals forces.[41] This scenario is sketched in Figure 2f and suggests that the crack opening becomes wider with slip between graphene monolayer and add-layer while the graphene add-layer remains well adhered to the copper foil. Stronger interactions are more likely to promote deflections of cracks in the monolayer, but this was not observed.

As the applied strain increased to 2.6% (Figure 2c), new cracks (Ⓓ, Ⓔ, Ⓕ, and Ⓖ) appeared between the existing cracks (Ⓐ, Ⓑ, and Ⓒ), making the overall crack spacing smaller. At the same time, the existing cracks became more visible, which suggests that their crack opening became wider. When the strain reached 3.7% (Figure 2d), only one new crack, Ⓗ, was observed and was accompanied by further opening of the other pre-existing cracks.

New wrinkles can also be seen, particularly when the region in the red box (Figure 2e) is magnified along with cracks Ⓑ, Ⓒ, and Ⓕ. They were not as clear as the initial wrinkles (Figure 2d) due to the fact that they were likely smaller and the noise in the SEM images increases with time due to the electron-beam-induced deposition of carbon contaminants on the specimen.[42,43] For this reason, a new region was chosen with 7000× magnification (Figure 2g) in order to emphasize the generation of new wrinkles parallel to the direction of loading. In this case, the applied strain was 7.2%. The appearance of the new wrinkles is due to the transverse strains generated by Poisson effects, which caused microbuckling of the graphene through compressive delamination.[44] It should be noted that the orientation of wrinkles formed during graphene growth is typically as random as the orientation of the copper grains,[45,46] likely caused by the mismatch of the coefficient of thermal expansion between graphene and copper.[47] The formation of new wrinkles is also consistent with observations of wrinkling in tensile experiments of graphene transferred to polymer substrates.[23] A magnified view (Figure 2h) of the region in the orange box (Figure 2g) clearly shows the presence of a crack in the monolayer graphene that was not deflected by the add-layer beneath it, nor was the add-layer penetrated by the crack. Furthermore, the presence of the add-layer did not deflect the crack, nor did it affect the crack opening in the monolayer. At the same time, the adhesion of the add-layer to the copper foil is expected to be as strong as that of monolayer graphene to copper foil.[32] These observations suggest that the adhesion between the add-layer and monolayer is relatively weak. Additionally, the small in-plane dimension of the add-layers does not allow much shear strain to be developed at the interface between them and copper.

Atomic force microscopy was performed to provide topological information (Figure 3) of the copper-supported graphene before and after the tension test. Figure 3a shows the initial state of the graphene surface after CVD growth. A series of copper steps are clearly visible. They are a result of the interaction between copper and graphene during the growth of graphene.[30,32] There is also a graphene wrinkle in the scanned area, and a height profile (Figure 3c) taken along line a−a (Figure 3a) indicates that its height was 3.3 nm while its width was approximately 100 nm. The cantilever used to make this

DOI: 10.1021/acsnano.6b05101
ACS Nano 2016, 10, 9616−9625

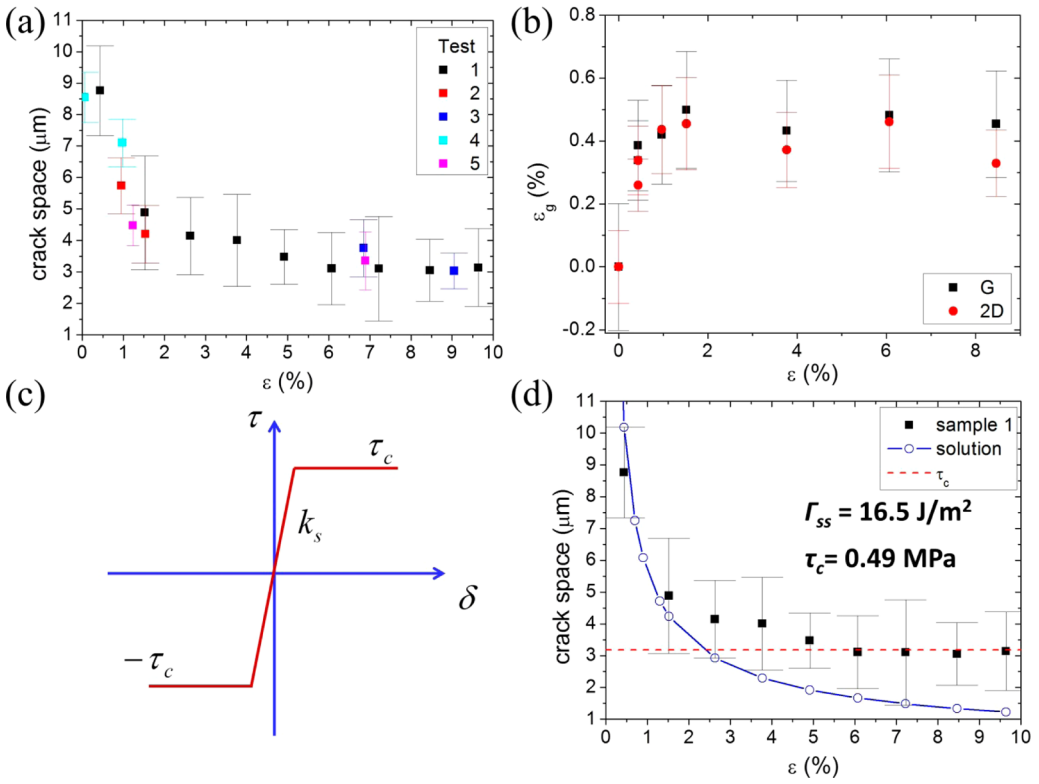

Figure 5. Fracture mechanics evaluation of graphene and its interface. (a) Crack spacing as the function of the applied strains, (b) transferred strains on graphene as a function of the applied tensile strain, (c) shear stress at the interface as the function of the relative displacement, and (d) evaluation of the fracture and interface response of graphene and its interface.

measurement was sharpened and has a local radius of curvature of approximately 10 nm. Due to tip convolution, we estimate that this effect makes the wrinkles appear 20−40 nm wider than they really are. The image (Figure 3b) taken at an applied strain of 10.8% indicates that the copper surface became rougher following yield, which is probably due to the out-of-plane slip of dislocations in the copper foil.[48] Due to the applied strain, new wrinkles appeared that were parallel to the direction of loading, and as indicated earlier, they were caused by the compressive transverse strain.[23] The profile (Figure 3c) along the line b−b (Figure 3b) of a typical wrinkle induced by the compressive transverse strain is similar in height to the wrinkle formed during CVD, but these new wrinkles were notably narrower at about 50 nm.

The presence of cracks and wrinkles in the graphene were also visualized by lateral force microscopy. This technique records the lateral tip deflection in traced and retraced AFM scans. The different tip behavior in these two scans can be generally interpreted as a measure of friction coefficient.[49] The scan in Figure 3d is a lateral force image of the same region shown in Figure 3b. The darker contrast corresponds to higher friction forces, which are attributed to exposed copper, while the brighter contrast corresponds to the low friction commonly associated with graphene.[50] The secondary wrinkles can again be observed running parallel to the loading direction. They hinder any further growth of the existing channel cracks. This is likely due to the fact that the wrinkles can relieve the strain at the tip of a propagating crack. Once a channel crack had initiated, its faces continued to open as the applied strain increased. For example, the maximum crack opening was approximately 500 nm (Figure 3d). This apparently uninhibited crack opening also suggests that the strength of the shear interaction between graphene and copper is quite weak. The friction force along the blue and red scan lines in Figure 3d is shown in Figure 3e. It can be seen that the friction force was indeed higher over the exposed copper and provided an unambiguous measure of the opening width of the crack in the graphene. The fact that the variation in height is the same in the two regions rules out the potential contribution of roughness to the friction measurements.

Raman spectroscopy (λ = 488 nm) was performed *ex situ* on the graphene-coated copper foil following unloading from several levels of applied strain. The Raman spectra of graphene provide a wealth of information such as crystalline quality, number of graphene layers, and the strain in the graphene. Figure 4a shows the graphene bands (G and 2D) at applied strains of 0, 0.44, and 3.7%. The full spectrum (Figure S3) does not display a D band at 1350 cm^{-1}, which indicates the absence of a significant number of defects.[51] The intensity ratio (I_{2D}/I_G) of the 2D and G peaks is 2.04, 2.27, and 2.14 at applied strain levels of 0, 0.44, and 3.7%, respectively. This confirms the presence of monolayer graphene. An even more interesting feature is the downshift of the G and 2D peaks as the applied strain increased. Such shifts can be produced not only by strain in graphene[21−25,52,53] but also by chemical doping[54] and the orientation of copper grains.[55] These potential sources can be separated by observing the form of the cross plot (Figure 4b) of the position of the 2D band and the G band. A linear response over the entire strain range was observed with a slope of approximately 1.8.[24] Such a linear response rules out chemical doping effects, which are usually associated with nonlinear behavior. The slope of the line can also be affected by the difference in orientation of the copper and graphene grains.[55] However, the orientation of grains in copper foil is generally

DOI: 10.1021/acsnano.6b05101
ACS Nano 2016, 10, 9616−9625

quite random and remains so as the applied strain is increased. Thus, such orientation effects should be negligible, and the shifts in the Raman peaks were indeed due to the strain in the monolayer graphene.

The positions of the G and 2D peaks were plotted as a function of the applied strain (Figure 4c,d). There is a noticeable dependence of the position of the peaks for very small strains as the peaks dropped from their initial values to approximately 1577 and 2699 cm^{-1} at an applied strain of about 0.44%. Beyond this, the positions of the G and 2D peaks stayed the same, which indicates that the applied strain on the copper foil is no longer being transferred to the graphene due to slippage. At lower strains (<0.44%), a linear relationship was observed between the positions of the G and 2D peaks and the applied strain. The slopes of the lines are -16.5 ± 6.2 and -31.1 ± 10.0 $cm^{-1}/\%$ for the G and 2D peaks, respectively. Both slopes are comparable to the response of single-walled nanotubes or graphene. The slopes for the G band have ranged from -11.7 to -20.2 $cm^{-1}/\%$, whereas -7.9 to -57.6 $cm^{-1}/\%$ has been associated with the 2D band.[24,56,57] We attributed the strain-dependent Raman shift to the fact that the phonon deformation potential of graphene depends linearly on the strain.[58−60] As a result, the Raman shift can be related to the strain by

$$\frac{\omega^0 - \omega}{\omega^0} = \gamma(\varepsilon_{xx} + \varepsilon_{yy}) = \gamma(1 - \nu)\varepsilon_{xx} \quad (1)$$

where ω^0 and ω are, respectively, the locations of the G or 2D peaks at zero and subsequent levels of the applied strain, ε_{xx} is the applied strain in the longitudinal direction, ε_{yy} is the transverse strain, ν is Poisson's ratio, and γ is the Güneisen parameter for graphene. Since there was no slip between the graphene and the copper below 0.44% strain (Figure 3c,d), the strains in the graphene and copper can be assumed to be the same. Thus, the Poisson's ratio of the copper foil (0.33) was used in eq 1 along with the applied strain to determine the Güneisen parameter associated with the G and 2D bands. The Güneisen parameter was determined by a linear fit of the Raman shifts up to the value of 0.44% strain in Figure 3c,d. The value of the Güneisen parameter for the G band was $\gamma_G = 1.55 \pm 0.58$ $cm^{-1}/\%$, whereas $\gamma_{2D} = 1.71 \pm 0.55$ $cm^{-1}/\%$ for the 2D band. Although the Güneisen parameters have not been determined before for graphene grown on seed copper substrates, the values are in line with those obtained for graphene on PET,[23,24,52,58,60−62] which were obtained up to applied strain levels of 0.8%. This completed the observation stage of the investigation.

The main data extracted from the SEM images (Figure 2) was the crack spacing in the graphene as a function of the applied strain. At each applied strain level, the average crack spacing (Figure 5a) was obtained from at least 20 locations within a field of view of 51×44 μm. The crack spacing in each of the noted tests was measured from an image at one location. In some the tests, a number of locations were considered in addition to the main one and yielded qualitatively similar spacing. This is borne out by the consistency of the data from case to case in Figure 5a. The degree of scatter in the data is driven by the random nature of defects (the different orientations of each grain, the grain boundaries themselves, triple junctions, wrinkles, *etc.*). All five samples that were tested exhibited similar responses, and in each case, two different regimes could be observed. Initially, there was a sharp decrease in the average crack spacing. Beyond about 1.5% strain, the crack spacing was no longer affected by the applied strain. Such behavior is common in situations where loads between components of a composite are transferred by shear.[63,64]

The average strain in the graphene ε_g (Figure 5b) was tracked from several locations as a function of the applied strain from the corresponding shifts in the G and 2D peaks[23,24,58,60] using the Güneisen parameter determined from eq 1. The strain in the graphene was obtained from Raman spectra that were taken at 15−20 locations. The strains plotted in Figure 5b are the average, and the error bars reflect one standard deviation. With the optical microscope used for the Raman spectroscopy, it was not possible to locate spots at the midpoints between cracks, which is where the shear transfer is most likely to be complete. Instead, the Raman spots were 1 μm apart and had a diameter of 300 nm, approximately. The minimum crack spacing was 2−4 μm. Thus, the spots were potentially interrogating any point between one crack and another, thereby encountering a range of shear transfer conditions and contributing to the uncertainty registered by the error bars.

There was a sharp increase in the strain in the graphene (ε_g) at low loads followed by a transition to an approximately constant value of 0.45%. Note that the strain levels in the graphene were slightly different depending on which of the peaks was used. This may be due to the fact that the G band tends to split into G^+ and G^- sub-bands while the 2D peak does not.[25,53] Although such splitting cannot be seen in Figure 4a, expanded views of the data (Figure S4) do exhibit some broadening of the peak. As a result of this broadening, there was more uncertainty in the strains obtained from the G peak, as is reflected in the error bars. The correspondence of strain in the graphene (Figure 5b) with applied strain and variations of crack spacing (Figure 5a) suggests that the strain in graphene reached its peak when the crack spacing reached steady state. The fracture of graphene and the characteristic spacing are now linked to the shear interaction between the graphene and copper using two shear-lag models, one for the initial response and the other for the constant crack spacing regime.

In view of the observations above, the shear interaction between graphene and copper can be idealized by an initially linearly elastic response followed by a constant shear strength for sliding (Figure 5c). The linearly elastic portion of the interaction leads to the sequential formation of channel cracks in the graphene, resulting in progressively smaller spacing between the cracks. This was the noted initial portion of the response in Figure 5a,b. Such a phenomenon has been analyzed[65] as the sequential formation of periodic channel cracks in an elastic thin film on a semi-infinite substrate subjected to a uniaxial tensile load. The energy release rate associated with a particular crack spacing L and applied strain ε is

$$G = \frac{E_{2D}\varepsilon^2}{\lambda h}[2\tanh(\lambda L/2) - \tanh(\lambda L)] \quad (2)$$

where E_{2D} is the in-plane stiffness of graphene (350 N/m), the inverse of λ is the reference length ($\sqrt{k_s/E_{2D}}$) defined by the interfacial shear stiffness (k_s) and the in-plane stiffness of graphene while h is the thickness (0.335 nm) of graphene. In the experiments conducted here, the energy release rate is the fracture toughness of the graphene Γ, which must be determined from the data. The other unknown parameter is k_s, the stiffness of the interaction. As indicated in the

DOI: 10.1021/acsnano.6b05101
ACS Nano 2016, 10, 9616−9625

Supporting Information (section 4), the stiffness was taken to be 1.3 TN/m^3 based on the data at the three largest values of spacing. As a reference, the corresponding value for graphene on polyethylene terephthalate[74] was 74 TN/m^3. The toughness was then determined by substituting Γ for G in eq 1 at the same values of spacing that were used to determine the stiffness and taking the average, which turned out to be 16.5 J/m^2. This value of toughness is close to the one given by Zhang[20] for free-standing CVD-grown graphene.

The effect of the stiffness of the interaction was obtained at small strains. At applied strains above 7% (Figure 5a), the crack spacing reached its lower limit, which corresponds to complete slip along the interface between the graphene and copper at the interfacial shear strength τ_c (Figure 5c). The minimum crack spacing (see the section on shear interaction parameters in the Supporting Information) is controlled by the in-plane modulus, the toughness, and thickness of the graphene as well as the interfacial shear strength through

$$L_{\min} = \left(\frac{4E_{2D}\Gamma h}{\tau_c^2}\right)^{1/3} \quad (3)$$

Using an average value of 3.18 μm for the minimum crack spacing and 16.5 J/m^2 for the toughness of the graphene set the shear strength at 0.49 MPa. This is about 1 order of magnitude stronger than the interlayer interactions in graphite[72] and reinforces the claim made earlier about the weak interaction between monolayer and add-layer graphene.

It should be noted that neither SEM, AFM, nor Raman spectroscopy was able to detect graphene defects on the copper strip. Nonetheless, the formation of channel cracks in graphene was initially observed at applied strains of approximately 0.44%. When graphene is grown on copper foil using chemical vapor deposition, growth is nucleated at randomly positioned sites and occurs in a radial manner until individual grains connect at grain boundaries. This growth mechanism does not produce line defects that could be construed as cracks. Instead, it is most likely that, upon loading, the cracks nucleated from triple junctions, where the stress concentrations are highest.

As a practical matter for roll-to-roll dry transfer of graphene, where it is likely to be subject to strain induced by the curvature of the rollers and/or tension applied to the composite film, the simplest objective would be to maintain applied strain levels to less than about 0.5%. If this is not possible, the presence of cracks is likely to increase the sheet resistance of the graphene. This could be viewed as an opportunity in some applications where the sheet resistance could be tuned by crack spacing. Alternatively, the effects of channel cracking induced by rolling could be mitigated by adding conductive nanowires.[4]

CONCLUSIONS

Although CVD of graphene on copper[66,67] has opened the door to large-area production of graphene, there is currently a bottleneck in production due to the fact that graphene can only be transferred to target substrates by etching away the copper[68,69] or electrochemically delaminating it.[70] These are both relatively slow and wasteful processes that make mechanical or dry transfer appealing. Following recent progress in selective dry transfer,[32] with its potential for scale up to roll-to-roll nanomanufacturing, the possibility of graphene fracture under the tensile loading that is inherent to such processes was addressed here. The tensile behavior of CVD-grown graphene was examined *via in situ* experiments in an SEM. Additional observations were carried out with AFM and Raman spectroscopy at selected load intervals.

The graphene began to develop channel cracking at an applied strain level of almost 0.5%, double the yield strength of the annealed seed copper. The crack spacing decreased with increasing applied strain until saturation occurred at about 6%. In addition, transverse wrinkling perpendicular to the channel cracks was clearly observed at an applied strain of about 2.6%. It was also noted that pre-existing wrinkles tended to arrest channel cracks. Raman spectroscopy confirmed that high-quality graphene had been grown on the copper foil. In addition, it was noted that the G and 2D peaks downshift with increasing applied strain. The Güneisen parameters were determined for each peak, which led to the conclusion that the highest strain in the graphene was 0.45%. This observation and the saturation in the crack spacing indicate that the graphene was sliding over the copper, which motivated simple models of shear transfer for the limiting behavior at small and large strains.

Accordingly, the shear interaction between graphene and its seed copper foil was modeled by an initial stiffness followed by a constant shear strength. The development of crack spacing in the linear regime was captured by a sequential cracking analysis.[65] When the measured crack spacing data were applied to this model, the stiffness of the interactions was 1.3 TN/m^3 and the fracture toughness of the graphene was 16.5 J/m^2. The measured saturation spacing was input to a simple shear-lag analysis based on a constant shear strength which turned out to be 0.49 MPa. This suggests that the adhesion interaction between graphene and copper foil is stronger than that of the interlayer graphene. These experiments suggest that cracking in graphene in roll-to-roll transfer can be avoided if the applied strain is less than about 0.5%. It remains to be seen how much cracking in graphene can be tolerated before its performance in the intended application starts to diminish.

EXPERIMENTS

An electrical discharge machine was used to form 130 μm thick bare copper foil into the shape shown in Figure S1b, whose dimensions are listed in Table S1. High-quality monolayer graphene was grown on the copper strips in a low-pressure chemical vapor deposition system.[8] The bare copper strips were placed in a 2 in. quartz tube, which was heated to 1035 °C. Hydrogen (H_2) was pumped through the system at a rate of 2 sccm and a pressure of 2.5 × 10^{-2} mbar. Once the temperature reached 1035 °C, the copper was annealed for 30 min in the hydrogen atmosphere. Methane (CH_4) was then introduced at 7 sccm at a pressure of 1.4 × 10^{-2} mbar for 10 min, followed by cooling to room temperature in 30 min.

Tensile tests were conducted using a Deben Microtest system, inside a FEI Quanta 600 FEG SEM. The graphene-coated strips were then mounted in the *in situ* tensile loading device that was placed in a SEM. The tensile tests were conducted in displacement control, while the load was measured by a 200 N load cell. In most of the experiments, the applied displacement was interrupted and fixed while the SEM images were taken. The images were used to determine the crack spacing as a function of applied strain. In some experiments, the specimens were removed from the loading device at several levels of applied strain to allow Raman spectra to be obtained. Micro-Raman measurements were made with a Witec model Alpha 300 scanning Raman system using 488 nm excitation. AFM measurements were made with a Park Scientific model Autoprobe CP, with a Bruker MSCT type A cantilever.

DOI: 10.1021/acsnano.6b05101
ACS Nano 2016, 10, 9616−9625

ASSOCIATED CONTENT

Supporting Information

The Supporting Information is available free of charge on the ACS Publications website at DOI: 10.1021/acsnano.6b05101.

In situ tensile testing, stress−strain behavior, Raman spectra, and shear interaction parameters (PDF)

AUTHOR INFORMATION

Corresponding Author

*E-mail: kml@mail.utexas.edu.

Author Contributions

§S.R.N. and X.W. contributed equally to this work.

Notes

The authors declare no competing financial interest.

ACKNOWLEDGMENTS

The authors gratefully acknowledge partial financial support of this work by the National Science Foundation through Grant No. CMMI-1130261. This work is also based upon work supported in part by the National Science Foundation under Cooperative Agreement No. EEC-1160494. Any opinions, findings, and conclusions or recommendations expressed in this material are those of the authors and do not necessarily reflect the views of the National Science Foundation. G.W. acknowledges support from the Rashid Engineering Regents Chair.

REFERENCES

(1) Bae, S.; Kim, H.; Lee, Y.; Xu, X.; Park, J.-S.; Zheng, Y.; Balakrishnan, J.; Lei, T.; Kim, H. R.; Song, Y. I.; et al. Roll-to-roll Production of 30-in. Graphene Films for Transparent Electrodes. *Nat. Nanotechnol.* **2010**, *5*, 574−578.

(2) Kobayashi, T.; Bando, M.; Kimura, N.; Shimizu, K.; Kadono, K.; Umezu, N.; Miyahara, K.; Hayazaki, S.; Nagai, S.; Mizuguchi, Y.; et al. Production of a 100-m-long High-quality Graphene Transparent Conductive Film by Roll-to-roll Chemical Vapor Deposition and Transfer process. *Appl. Phys. Lett.* **2013**, *102*, 023112.

(3) Chandrashekar, B. N.; Deng, B.; Smitha, A. S.; Chen, Y.; Tan, C.; Zhang, H.; Peng, H.; Liu, Z. Roll-to-roll Green Transfer of CVD Graphene onto Plastic for a Transparent and Flexible Triboelectric Nanogenerator. *Adv. Mater.* **2015**, *27*, 5210−5216.

(4) Deng, B.; Hsu, P.-C.; Chen, G.; Chandrashekar, B.; Liao, L.; Ayitimuda, Z.; Wu, J.; Guo, Y.; Lin, L.; Zhou, Y.; et al. Roll-to-roll Encapsulation of Metal Nanowires between Graphene and Plastic Substrate for High-performance Flexible Transparent Electrodes. *Nano Lett.* **2015**, *15*, 4206−4213.

(5) Wang, X.; Zhi, L. J.; Mullen, K. Transparent, Conductive Graphene Electrodes for Dye-sensitized Solar Cells. *Nano Lett.* **2008**, *8*, 323−327.

(6) Cohen-Tanugi, D.; Grossman, J. C. Water Desalination across Nanoporous Graphene. *Nano Lett.* **2012**, *12*, 3602−3608.

(7) Peplow, M. Graphene Booms in Factories but Lacks a Killer App. *Nature* **2015**, *522*, 268−269.

(8) Li, X.; Cai, W.; An, J.; Kim, S.; Nah, J.; Yang, D.; Piner, R.; Velamakanni, A.; Jung, I.; Tutuc, E.; et al. Large-area Synthesis of High-quality and Uniform Graphene Films on Copper Foils. *Science* **2009**, *324*, 1312−1314.

(9) Li, X. S.; Zhu, Y. W.; Cai, W. W.; Borysiak, M.; Han, B. Y.; Chen, D.; Piner, R. D.; Colombo, L.; Ruoff, R. S. Transfer of Large-area Graphene Films for High-performance Transparent Conductive Electrodes. *Nano Lett.* **2009**, *9*, 4359−4363.

(10) Wang, Y.; Zheng, Y.; Xu, X.; Dubuisson, E.; Bao, Q.; Lu, J.; Loh, K. P. Electrochemical Delamination of CVD-grown Graphene Film: Toward the Recyclable Use of Copper Catalyst. *ACS Nano* **2011**, *5*, 9927−9933.

(11) Morse, J. *Nanofabrication Technologies for Roll-to-roll Processing*; Workshop on Nanofabrication Technologies for Roll-to-Roll Processing, Boston, MA, September 27−28, 2011.

(12) Polsen, E. S.; McNerny, D. Q.; Viswanath, B.; Pattinson, S. W.; Hart, A. J. High-speed Roll-to-roll manufacturing of Graphene Using a Concentric Tube CVD Reactor. *Sci. Rep.* **2015**, *5*, 10257.

(13) Lee, C.; Wei, X.; Kysar, J. W.; Hone, J. Measurement of the Elastic Properties and Intrinsic Strength of Monolayer Graphene. *Science* **2008**, *321*, 385−388.

(14) Jiang, J.-W.; Wang, J.-S.; Li, B. Young's modulus of Graphene: a Molecular Dynamics Study. *Phys. Rev. B: Condens. Matter Mater. Phys.* **2009**, *80*, 113405.

(15) Kotakoski, J.; Meyer, J. C. Mechanical Properties of Polycrystalline Graphene Based on a Realistic Atomistic Model. *Phys. Rev. B: Condens. Matter Mater. Phys.* **2012**, *85*, 195447.

(16) Hajgató, B. z.; Güryel, S. l.; Dauphin, Y.; Blairon, J.-M.; Miltner, H. E.; Van Lier, G.; De Proft, F.; Geerlings, P. Theoretical Investigation of the Intrinsic Mechanical Properties of Single-and Double-layer Graphene. *J. Phys. Chem. C* **2012**, *116*, 22608−22618.

(17) Pereira, V. M.; Castro Neto, A. H.; Peres, N. M. R. Tight-binding Approach to Uniaxial Strain in Graphene. *Phys. Rev. B: Condens. Matter Mater. Phys.* **2009**, *80*, 045401.

(18) Huang, P. Y.; Ruiz-Vargas, C. S.; van der Zande, A. M.; Whitney, W. S.; Levendorf, M. P.; Kevek, J. W.; Garg, S.; Alden, J. S.; Hustedt, C. J.; Zhu, Y.; et al. Grains and Grain Boundaries in Single-layer Graphene Atomic Patchwork Quilts. *Nature* **2011**, *469*, 389−392.

(19) Kim, K.; Lee, Z.; Regan, W.; Kisielowski, C.; Crommie, M.; Zettl, A. Grain Boundary Mapping in Polycrystalline graphene. *ACS Nano* **2011**, *5*, 2142−2146.

(20) Zhang, P.; Ma, L.; Fan, F.; Zeng, Z.; Peng, C.; Loya, P. E.; Liu, Z.; Gong, Y.; Zhang, J.; Zhang, X. Fracture Toughness of Graphene. *Nat. Commun.* **2014**, *5*, 3782.

(21) Tsoukleri, G.; Parthenios, J.; Papagelis, K.; Jalil, R.; Ferrari, A. C.; Geim, A. K.; Novoselov, K. S.; Galiotis, C. Subjecting a Graphene Monolayer to Tension and Compression. *Small* **2009**, *5*, 2397−2402.

(22) Gong, L.; Kinloch, I. A.; Young, R. J.; Riaz, I.; Jalil, R.; Novoselov, K. S. Interfacial Stress Transfer in a Graphene Monolayer Nanocomposite. *Adv. Mater.* **2010**, *22*, 2694−2697.

(23) Jiang, T.; Huang, R.; Zhu, Y. Interfacial Sliding and Buckling of Monolayer Graphene on a Stretchable Substrate. *Adv. Funct. Mater.* **2014**, *24*, 396−402.

(24) Anagnostopoulos, G.; Androulidakis, C.; Koukaras, E. N.; Tsoukleri, G.; Polyzos, I.; Parthenios, J.; Papagelis, K.; Galiotis, C. Stress Transfer Mechanisms at the Submicron Level for Graphene/Polymer Systems. *ACS Appl. Mater. Interfaces* **2015**, *7*, 4216−4223.

(25) del Corro, E.; Kavan, L.; Kalbac, M.; Frank, O. Strain Assessment in Graphene through the Raman 2D′ mode. *J. Phys. Chem. C* **2015**, *119*, 25651−25656.

(26) Liu, N.; Pan, Z.; Fu, L.; Zhang, C.; Dai, B.; Liu, Z. The Origin of Wrinkles on Transferred Graphene. *Nano Res.* **2011**, *4*, 996−1004.

(27) Hao, Y.; Wang, L.; Liu, Y.; Chen, H.; Wang, X.; Tan, C.; Nie, S.; Suk, J. W.; Jiang, T.; Liang, T.; et al. Oxygen-activated Growth and Bandgap Tunability of Large Single-crystal Bilayer Graphene. *Nat. Nanotechnol.* **2016**, *11*, 426.

(28) Li, Q.; Chou, H.; Zhong, J.-H.; Liu, J.-Y.; Dolocan, A.; Zhang, J.; Zhou, Y.; Ruoff, R. S.; Chen, S.; Cai, W. Growth of Adlayer Graphene on Cu Studied by Carbon Isotope Labeling. *Nano Lett.* **2013**, *13*, 486−490.

(29) Mattevi, C.; Kim, H.; Chhowalla, M. A Review of Chemical Vapour Deposition of Graphene on Copper. *J. Mater. Chem.* **2011**, *21*, 3324−3334.

(30) Wang, Z.-J.; Weinberg, G.; Zhang, Q.; Lunkenbein, T.; Klein-Hoffmann, A.; Kurnatowska, M.; Plodinec, M.; Li, Q.; Chi, L.; Schloegl, R.; et al. Direct Observation of Graphene Growth and Associated Copper Substrate Dynamics by *in-situ* Scanning Electron Microscopy. *ACS Nano* **2015**, *9*, 1506−1519.

(31) Xie, C.; Tong, W. Cracking and Decohesion of a Thin Al_2O_3 Film on a Ductile Al−5% Mg Aubstrate. *Acta Mater.* **2005**, *53*, 477−485.

DOI: 10.1021/acsnano.6b05101
ACS Nano 2016, 10, 9616−9625

(32) Na, S. R.; Suk, J. W.; Tao, L.; Akinwande, D.; Ruoff, R. S.; Huang, R.; Liechti, K. M. Selective Mechanical Transfer of Graphene from Seed Copper Foil Using Rate Effects. *ACS Nano* **2015**, *9*, 1325−1335.
(33) Topsakal, M.; Ciraci, S. Elastic and Plastic Deformation of Graphene, Silicene, and Boron Nitride Honeycomb Nanoribbons under Uniaxial Tension: A first-principles density-functional theory study. *Phys. Rev. B: Condens. Matter Mater. Phys.* **2010**, *81*, 024107.
(34) Zhao, H.; Min, K.; Aluru, N. Size and Chirality Dependent Elastic Properties of Graphene Nanoribbons under Uniaxial Tension. *Nano Lett.* **2009**, *9*, 3012−3015.
(35) Song, Z.; Artyukhov, V. I.; Yakobson, B. I.; Xu, Z. Pseudo Hall−Petch Strength Reduction in Polycrystalline Graphene. *Nano Lett.* **2013**, *13*, 1829−1833.
(36) Sha, Z.; Pei, Q.; Liu, Z.; Shenoy, V.; Zhang, Y. Is the Failure of Large-area Polycrystalline Graphene Notch Sensitive or Insensitive? *Carbon* **2014**, *72*, 200−206.
(37) Sha, Z.; Quek, S.; Pei, Q.; Liu, Z.; Wang, T.; Shenoy, V.; Zhang, Y. Inverse Pseudo Hall-Petch Relation in Polycrystalline Graphene. *Sci. Rep.* **2014**, *4*, 05991.
(38) Sha, Z.; Wan, Q.; Pei, Q.; Quek, S.; Liu, Z.; Zhang, Y.; Shenoy, V. On the Failure Load and Mechanism of Polycrystalline Graphene by Nanoindentation. *Sci. Rep.* **2014**, *4*, 7437.
(39) Koren, E.; Lörtscher, E.; Rawlings, C.; Knoll, A. W.; Duerig, U. Adhesion and Friction in Mesoscopic Graphite Contacts. *Science* **2015**, *348*, 679−683.
(40) Soule, D.; Nezbeda, C. Direct Basal-plane Shear in Single-crystal Graphite. *J. Appl. Phys.* **1968**, *39*, 5122−5139.
(41) Geim, A. K.; Grigorieva, I. V. Van der Waals Heterostructures. *Nature* **2013**, *499*, 419−425.
(42) Zaitsev, S.; Shtempluck, O.; Buks, E. Effects of Electron Beam Induced Carbon Deposition on the Mechanical Properties of a Micromechanical Oscillator. *Sens. Actuators, A* **2012**, *179*, 237−241.
(43) Reimer, L. *Scanning Electron Microscopy: Physics of Image Formation and Microanalysis*; Springer: Berlin, 1985.
(44) Chai, H.; Babcock, C. D.; Knauss, W. G. One Dimensional Modelling of Failure in Laminated Plates by Delamination Buckling. *Int. J. Solids Struct.* **1981**, *17*, 1069−1083.
(45) He, R.; Zhao, L.; Petrone, N.; Kim, K. S.; Roth, M.; Hone, J.; Kim, P.; Pasupathy, A.; Pinczuk, A. Large Physisorption Strain in Chemical Vapor Deposition of Fraphene on Copper Substrates. *Nano Lett.* **2012**, *12*, 2408−2413.
(46) Zhang, Y.; Gao, T.; Gao, Y.; Xie, S.; Ji, Q.; Yan, K.; Peng, H.; Liu, Z. Defect-like Structures of Graphene on Copper Foils for Strain Relief Investigated by High-resolution Scanning Tunneling Microscopy. *ACS Nano* **2011**, *5*, 4014−4022.
(47) Hattab, H.; N'Diaye, A. T.; Wall, D.; Klein, C.; Jnawali, G.; Coraux, J.; Busse, C.; van Gastel, R.; Poelsema, B.; Michely, T.; et al. Interplay of Wrinkles, Strain, and Lattice Parameter in Graphene on Iridium. *Nano Lett.* **2012**, *12*, 678−682.
(48) Hall, E. The Deformation and Ageing of Mild Steel: III Siscussion of Results. *Proc. Phys. Soc., London, Sect. B* **1951**, *64*, 747.
(49) Marsden, A. J.; Phillips, M.; Wilson, N. R. Friction Force Microscopy: a Simple Technique for Identifying Graphene on Rough Substrates and Mapping the Orientation of Graphene Grains on Copper. *Nanotechnology* **2013**, *24*, 255704.
(50) Egberts, P.; Han, G. H.; Liu, X. Z.; Johnson, A. C.; Carpick, R. W. Frictional Behavior of Atomically Thin Sheets: Hexagonal-shaped Graphene Islands Grown on Copper by Chemical Vapor Deposition. *ACS Nano* **2014**, *8*, 5010−5021.
(51) Ferrari, A.; Meyer, J.; Scardaci, V.; Casiraghi, C.; Lazzeri, M.; Mauri, F.; Piscanec, S.; Jiang, D.; Novoselov, K.; Roth, S.; et al. Raman Spectrum of Graphene and Graphene Layers. *Phys. Rev. Lett.* **2006**, *97*, 187401.
(52) Ding, F.; Ji, H.; Chen, Y.; Herklotz, A.; Dörr, K.; Mei, Y.; Rastelli, A.; Schmidt, O. G. Stretchable graphene: A Close Look at Fundamental Parameters through Biaxial Straining. *Nano Lett.* **2010**, *10*, 3453−3458.
(53) Polyzos, I.; Bianchi, M.; Rizzi, L.; Koukaras, E. N.; Parthenios, J.; Papagelis, K.; Sordan, R.; Galiotis, C. Suspended Monolayer Graphene under True Uniaxial Deformation. *Nanoscale* **2015**, *7*, 13033−13042.
(54) Moldt, T.; Eckmann, A.; Klar, P.; Morozov, S. V.; Zhukov, A. A.; Novoselov, K. S.; Casiraghi, C. High-yield Production and Transfer of Graphene Flakes Obtained by Anodic bonding. *ACS Nano* **2011**, *5*, 7700−7706.
(55) Frank, O.; Vejpravova, J.; Holy, V.; Kavan, L.; Kalbac, M. Interaction between Graphene and Copper substrate: The Role of Lattice Orientation. *Carbon* **2014**, *68*, 440−451.
(56) Cronin, S.; Swan, A.; Ünlü, M.; Goldberg, B.; Dresselhaus, M.; Tinkham, M. Resonant Raman Spectroscopy of Individual Metallic and Semiconducting Single-wall Carbon Nanotubes under Uniaxial strain. *Phys. Rev. B: Condens. Matter Mater. Phys.* **2005**, *72*, 035425.
(57) Cooper, C.; Young, R. Investigation of Structure/property Relationships in Particulate Composites through the Use of Raman Spectroscopy. *J. Raman Spectrosc.* **1999**, *30* (10), 929−938.
(58) Ni, Z. H.; Yu, T.; Lu, Y. H.; Wang, Y. Y.; Feng, Y. P.; Shen, Z. X. Uniaxial Strain on Graphene: Raman Spectroscopy Study and Band-gap Opening. *ACS Nano* **2008**, *2*, 2301−2305.
(59) Huang, M.; Yan, H.; Chen, C.; Song, D.; Heinz, T. F.; Hone, J. Phonon Softening and Crystallographic Orientation of Strained Graphene Studied by Raman Spectroscopy. *Proc. Natl. Acad. Sci. U. S. A.* **2009**, *106*, 7304−7308.
(60) Mohiuddin, T.; Lombardo, A.; Nair, R.; Bonetti, A.; Savini, G.; Jalil, R.; Bonini, N.; Basko, D.; Galiotis, C.; Marzari, N.; et al. Uniaxial Strain in Graphene by Raman Spectroscopy: G Peak Splitting, Grüneisen Parameters, and Sample Orientation. *Phys. Rev. B: Condens. Matter Mater. Phys.* **2009**, *79*, 205433.
(61) Zabel, J.; Nair, R. R.; Ott, A.; Georgiou, T.; Geim, A. K.; Novoselov, K. S.; Casiraghi, C. Raman Spectroscopy of Graphene and Bilayer under Biaxial Strain: Bubbles and Balloons. *Nano Lett.* **2012**, *12*, 617−621.
(62) Ferralis, N. Probing Mechanical Properties of Graphene with Raman Spectroscopy. *J. Mater. Sci.* **2010**, *45*, 5135−5149.
(63) Piggott, M. Debonding and Friction at Fibre-polymer Interfaces. I: Criteria for Failure and Sliding. *Compos. Sci. Technol.* **1987**, *30*, 295−306.
(64) Crossman, F.; Wang, A. The Dependence of Transverse Cracking and Delamination on Ply Thickness in Graphite/Epoxy Laminates. *Damage in Composite Materials: Basic Mechanisms, Accumulation, Tolerance, and Characterization*; ASTM International: West Conshohocken, PA, 1982.
(65) Xia, Z. C.; Hutchinson, J. W. Crack Patterns in Thin Films. *J. Mech. Phys. Solids* **2000**, *48*, 1107−1131.
(66) Reina, A.; Jia, X.; Ho, J.; Nezich, D.; Son, H.; Bulovic, V.; Dresselhaus, M. S.; Kong, J. Large Area, Few-layer Graphene Films on Arbitrary Substrates by Chemical Vapor Deposition. *Nano Lett.* **2009**, *9*, 30−35.
(67) Li, X.; Magnuson, C. W.; Venugopal, A.; Tromp, R. M.; Hannon, J. B.; Vogel, E. M.; Colombo, L.; Ruoff, R. S. Large-area Graphene Single Crystals Grown by Low-pressure Chemical Vapor Deposition of Methane on Copper. *J. Am. Chem. Soc.* **2011**, *133*, 2816−2819.
(68) Na, S. R.; Suk, J. W.; Ruoff, R. S.; Huang, R.; Liechti, K. M. Ultra Long-range Interactions Between Large Area Graphene and Silicon. *ACS Nano* **2014**, *8*, 11234−11242.
(69) Suk, J. W. Fabrication and Mechanical Characterization of Graphene Based Membranes and Their Use in Thermoacoustics. University of Texas, Austin, TX, 2011; pp 1 online resource; https://repositories.lib.utexas.edu/bitstream/handle/2152/ETD-UT-2011-12-4653/SUK-DISSERTATION.pdf. Accessed 9/26/2016.
(70) Wang, X.; Tao, L.; Hao, Y.; Liu, Z.; Chou, H.; Kholmanov, I.; Chen, S.; Tan, C.; Jayant, N.; Yu, Q.; et al. Direct Delamination of Graphene for High-performance Plastic Electronics. *Small* **2014**, *10*, 694−698.
(71) Ambrosi, A.; Bonanni, A.; Sofer, Z.; Pumera, M. Large-scale Quantification of CVD Graphene Surface Coverage. *Nanoscale* **2013**, *5*, 2379−2387.

DOI: 10.1021/acsnano.6b05101
ACS Nano 2016, 10, 9616−9625

(72) Soule, D.; Nezbeda, C. Direct Basal-Plane Shear in Single-Crystal Graphite. *J. Appl. Phys.* **1968**, *39*, 5122−5139.
(73) Joshi, R.; Alwarappan, S.; Yoshimura, M.; Sahajwalla, V.; Nishina, Y. Graphene Oxide: the New Membrane Material. *Applied Materials Today* **2015**, *1*, 1−12.
(74) Guo, G.; Zhu, Y. Cohesive-Shear-Lag Modeling of Interfacial Stress Transfer Between a Monolayer Graphene and a Polymer Substrate. *J. Appl. Mech.* **2015**, *82*, 031005.

DOI: 10.1021/acsnano.6b05101
ACS Nano 2016, 10, 9616−9625